Process Safety and Environmental Protection 177 (2023) 1234–1248

Contents lists available at ScienceDirect

Process Safety and Environmental Protection

journal homepage: www.journals.elsevier.com/process-safety-and-environmental-protection

Substitution of diesel fuel in conventional compression ignition engine with waste biomass-based fuel and its validation using artificial neural networks

Krishnamoorthy Ramalingam [a,*], Elumalai Perumal Venkatesan [b], Suresh Vellaiyan [c,*], Azfarizal Mukhtar [d], Mohsen Sharifpur [e,f,**], Ahmad Shah Hizam Md Yasir [g], C Ahamed Saleel [h]

[a] Department of Mechanical Engineering, CK College of Engineering and Technology, Cuddalore, Tamil Nadu, India
[b] Department of Mechanical Engineering, Aditya Engineering College, Surampalem, India
[c] Department of Sustainable Engineering, Saveetha School of Engineering, SIMATS, Chennai, Tamil Nadu, India
[d] Institute of Sustainable Energy, Putrajaya Campus, Universiti Tenaga Nasional, Jalan IKRAM-UNITEN, 43000 Kajang, Malaysia
[e] Department of Mechanical and Aeronautical Engineering, University of Pretoria, Pretoria 0002, South Africa
[f] Department of Medical Research, China Medical University Hospital, China Medical University, Taichung, Taiwan
[g] Faculty of Resilience , Rabdan Academy, 65, Al Inshirah, Al Sa'adah, Abu Dhabi, 22401, PO Box: 114646, Abu Dhabi, UAE
[h] Department of Mechanical Engineering, College of Engineering, King Khalid University, PO Box 394, Abha 61421, Saudi Arabia

ARTICLE INFO

Keywords:
Waste to energy
Nano additive
Peel oil
Lather fat oil
NOx emission

ABSTRACT

This study aims to derive bioenergy from waste lather fat and citronella grass. Lather fat oil (LFO), citronella grass oil (CGO), a mixture of leather fat oil and citronella grass oil (LFCGO), and a nano-additive-incorporated mixture of lather fat oil and citronella grass oil (NFCO) were synthesized and used in diesel engines as the novelty of this study. ASTM standards were used to investigate and guarantee the fuel's properties. According to the experimental report, the nanoadditive's brake thermal efficiency and brake-specific fuel consumption were more comparable to diesel fuel. Compared to diesel, the NFCO blend reduced hydrocarbon, carbon monoxide, and particulate emissions by 6.48%, 12.33%, and 16.66%, respectively, while carbon dioxide and oxides of nitrogen emissions increased. The experiment's outcomes were verified using an artificial neural network (ANN). The trained model exhibits a remarkable coefficient of determination of 98%, with high R values varying from 0.9075 to 0.9998 and low mean absolute percentage error values ranging from 0.97% to 4.24%. Based on the experimental findings and validation report, it can be concluded that NFCO is an efficient diesel fuel substitute.

1. Introduction

Energy insecurity and waste disposal are two major global hazards to human life. Converting waste into energy is an option for circumventing these obstacles (Kurczyński et al., 2022). Since the 1980 s, diesel crops have replaced food crops, resulting in a food shortage. As a result, non-edible oil was chosen as a substitute fuel to reduce energy insecurity (Vigneswaran et al., 2018; Dhinesh et al., 2018a). Numerous nations around the globe are increasing pollution protections and adapting emission standards while recognizing the need to utilize alternative fuels (Subramani et al., 2018; Ramalingam et al., 2018). Previously, investigators replaced diesel with vegetable oil. Today, rather than vegetable oil, residual animal fats, non-edible seeds, biomass, leaves, resins, and vegetation are identified as the most cost-effective feedstocks for edible oil production (Parthasarathy et al., 2020; Perumal Venkatesan et al., 2019). Among these wastes, leather fat is the most cost-effective raw material for alternative energy and for reducing waste leather fat disposal, which substantially impacts the environment (Simsek and Uslu, 2020; Alptekin et al., 2015). However, its effectiveness is diminished when used in diesel engines that have yet to be modified. It is necessary to identify and evaluate additives capable of altering this biodiesel's physicochemical properties, such as its density, viscosity, and surface tension (Parthasarathy et al., 2021; Vellaiyan et al., 2021). Yuvarajan et al (Devarajan et al., 2022a). investigated the physico-thermal properties of waste lather fat oil and concluded that only the methyl ester met ASTM specifications for physico-thermal properties. The viscosity of unprocessed animal fat oil was detrimental to diesel engines, decreasing their efficiency, causing carbon deposition, etc (Vellaiyan and Partheeban, 2020). The transesterification procedure

* Corresponding author.
** Corresponding author at: Department of Mechanical and Aeronautical Engineering, University of Pretoria, Pretoria 0002, South Africa.
E-mail addresses: kskrishnamech@gmail.com (K. Ramalingam), suresh.vellaiyan@gmail.com (S. Vellaiyan), mohsen.sharifpur@up.ac.za (M. Sharifpur).

https://doi.org/10.1016/j.psep.2023.07.085
Received 4 April 2023; Received in revised form 23 July 2023; Accepted 28 July 2023
Available online 29 July 2023

Nomenclature

CI	Compression Ignition.
CV	Calorific value.
CN	Cetane Number.
CO	Carbon monoxide.
NO_x	Oxides of Nitrogen.
CO_2	Carbon dioxide.
HC	Hydro Carbon.
BSEC	Brake Specific Energy Consumption.
BTE	Brake Thermal Efficiency.
ASTM	American Society for Testing and Materials.
BP	Brake power.
ANN	Artificial neural network.
HSU	Hart ridge Smoke Units.
LGO	Lemon Grass Oil.
WCO	Waste Cooking Oil.
GC-MS	Gas Chromatography-Mass Spectrometry.
FT-IR	Fourier Transform Infrared spectroscopy.
MSE	Mean Square Error.
MAPE	Mean Absolute Percentage Error.

(Sivalingam et al., 2019), which converts crude oil to methyl ester using alcohol and additives, significantly improved the biodiesel's properties. According to the investigation, the methyl ester of waste animal fat oil efficiently powers a diesel engine (Barrios et al., 2014). However, all biodiesel blends had reduced HC, CO, and smoke emissions, which could explain why mixtures have a higher oxygen content. According to the research, waste animal fat biodiesel mixtures produce fewer emissions but higher NOx levels (Lapuerta et al., 2009).

The researcher (Altun and FevziYaşşar, 2013) demonstrated that the decreased energy content of waste-lather fat methyl ester biodiesel decreased its engine performance. Because transesterification is an alcoholic process, transesterified oil typically contains less energy than crude oil (Keskin et al., 2020). Recent experiments have shown that combining low-viscosity oil with unprocessed biofuel enhances engine efficiency relative to transesterified oil (Dubey and Gupta, 2017). The investigator examined a DI-CI engine that operated on a blend of unprocessed jatropha and low-viscosity turpentine oil. Compared to unprocessed jatropha oil and jatropha biodiesel, the mixed mixture was found to provide superior engine efficiency and emission formation. This may be the result of improved atomization and mixture penetration (Dubey and Gupta, 2018). Only the lemon peel oil with minimal viscosity was found to be affected by NOx (Ashok et al., 2018). The author investigated the use of diesel-citronella blends in diesel engines; all citronella blends emitted more NOx than diesel fuel alone (Senthur et al., 2022). When using biodiesel or biofuel in diesel engines, NOx emissions are typically elevated. This could be because of a link between the structure of fatty acids, a high cetane number, a decrease in the number of unsaturated compounds, or a shorter chain length in an alkyl ester (Nachippan et al., 2022).

This study examines diesel engines that utilize B100 fuel, which is comprised of 50% eucalyptus oil and 50% blended methyl ester of paradise oil. The effectiveness and emission metrics of the B100 blend were superior. In contrast, NOx pollution presented the greatest threat. The principal issue with plant-based fuels is NOx emissions (Devan and Mahalakshmi, 2009). Alcohol, water (for emulsion fuel), gasoline (for dual fuel mode), and nanoadditives (Nanofluids) were among the alternatives for minimizing NOx production (Senthilkumar et al., 2022). According to the researcher, adding nanomaterials (nanofluid) to the EGR system of an engine is the most effective way to simultaneously reduce NOx, HC, and CO emissions. This experiment added nanoparticles of cerium oxide to the propellant, lemongrass oil. It significantly enhanced the performance and responsiveness of the emission output. Due to their high surface area-to-volume ratio, nanofluids simultaneously reduce exhaust emissions (Vellaiyan, 2020). The composition of this work was inspired by interference. The waste lather oil was extracted from leather factory waste fat; it was then combined with citronella biodiesel, which was extracted by steam distillation, and tested in a diesel engine in various proportions.

2. Material and methods

2.1. Test fuel production

This study utilized citronella oil and residual lather fat oil as test fuel. Figs. 1 and 2 illustrate the production process in detail. Producing waste leather fat oil requires unprocessed skin, shorn hide, and waste flesh from the leather industry. Two stages are required to produce lather fat oil (LFO): hydrolysis and acid treatment (Lazaroiu et al., 2017). At a temperature of 110 °C, waste leather tissue, raw skin, and shaving hide

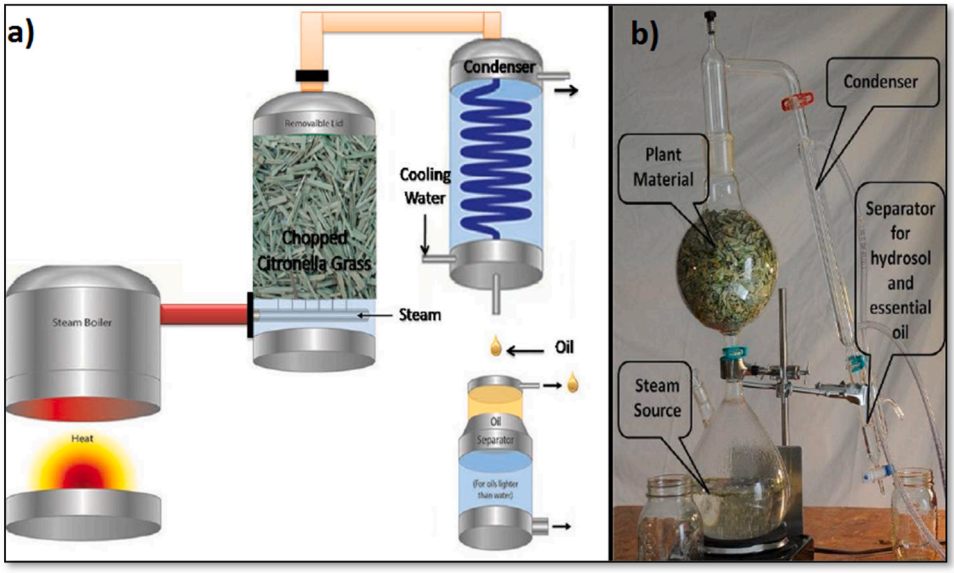

Fig. 1. Extraction of citronella oil (Ramalingam et al., 2020).

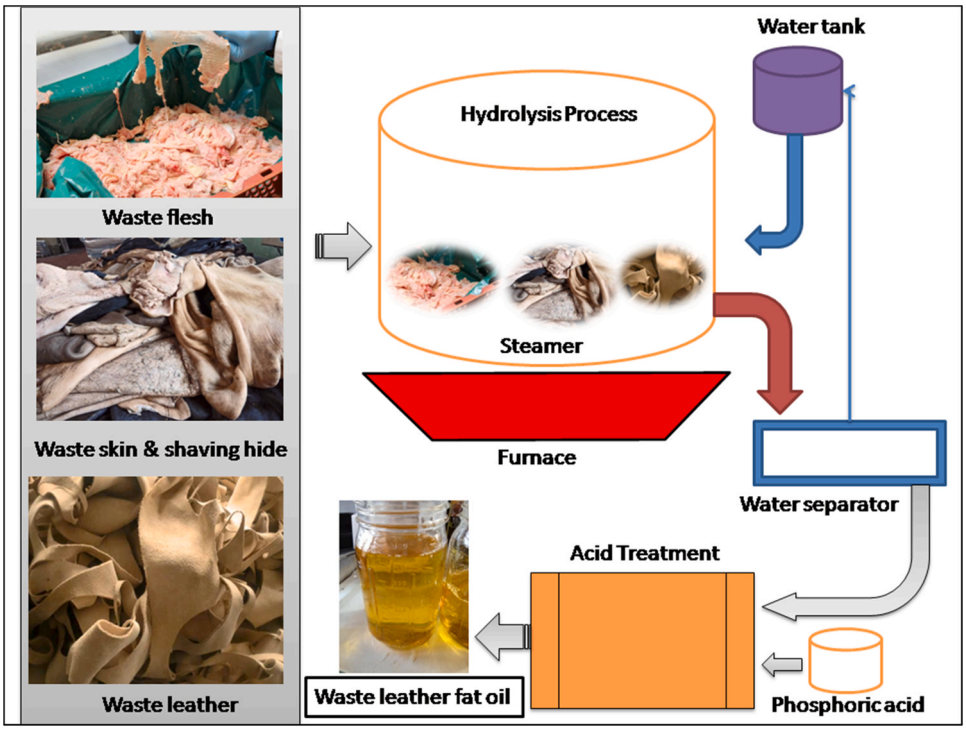

Fig. 2. Extraction of waste leather fat oil.

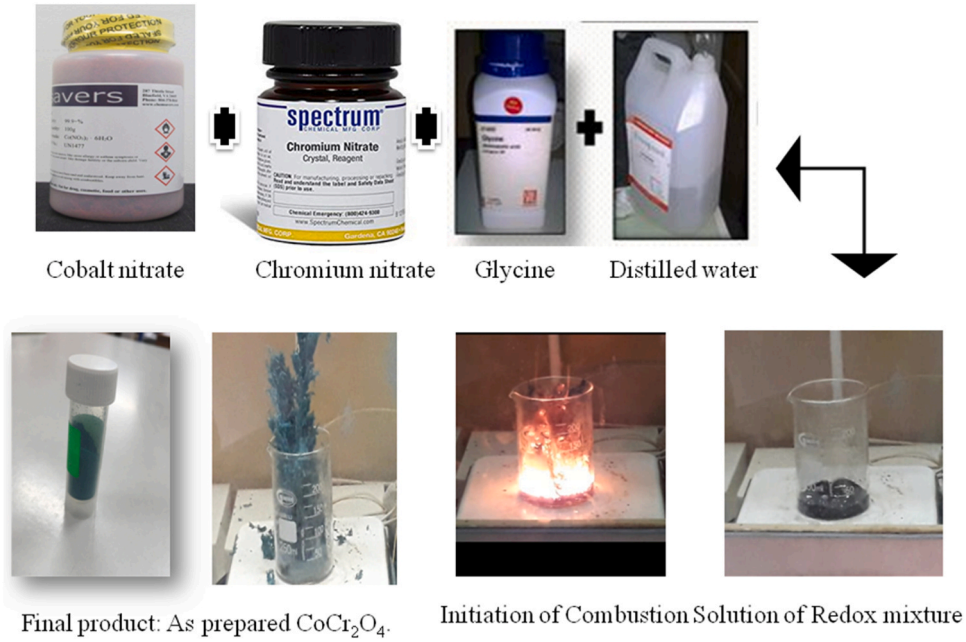

Fig. 3. Extraction of cobalt chromite.

are mixed with water in a ratio of 1:2 at a ratio of 1:2. This process facilitates the decomposition of proteinaceous substances and the formation of leather fat oil, which is then acid-treated to remove impurities such as tannins and other residues. Fig. 2 depicts the impurities that were eliminated by applying phosphoric acid at 60 °C for 15 min in this procedure. As described in our earlier study (Ramalingam et al., 2020), the citronella fuel was extracted through steam distillation.

2.2. Production of cobalt chromite nano additives

$CoCr_2O_4$ (cobalt chromite) was synthesized using simple combustion (SC) technology in the current study. The three stages of this process were the redox solution at 250 °C, the start of combustion, and the end product. 50 g of cobalt and chromium nitrates were combined with 10 g of glycine in a glass vial. From the total number of oxidation results of the oxidizer, the ratio of cobalt and chromium nitrates to glycine in the first mixture was calculated. To generate a 3 g batch of CoCr2O4, sufficient quantities of each reactant were dissolved in 100 ml of water to

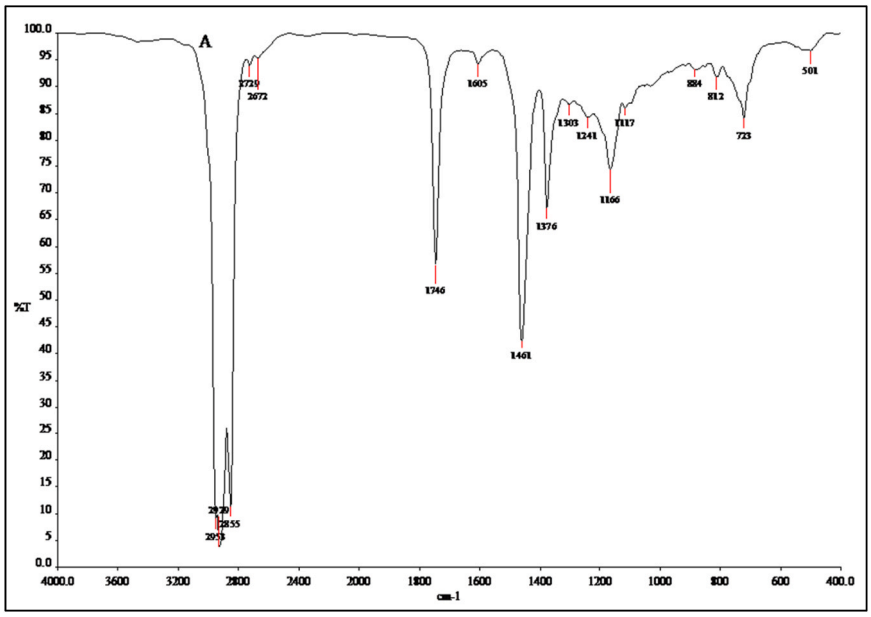

Fig. 4. FT-IR analysis of proposed fuel (Ramalingam et al., 2020).

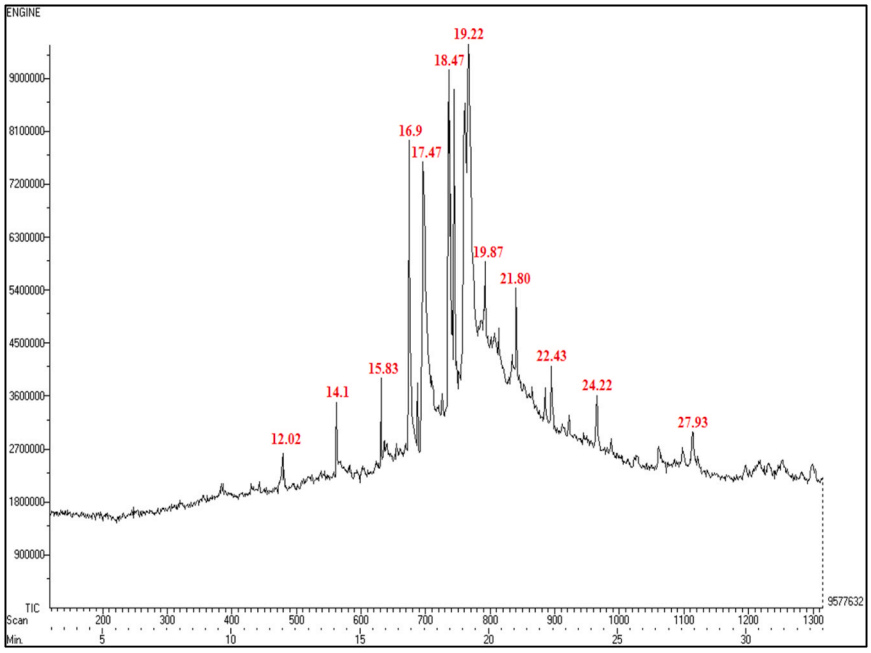

Fig. 5. GC-MS analysis of proposed fuel (Ramalingam et al., 2020).

form a homogenous solution. After the hydration, 6.8-pH water was used to dissolve it. The pH had a minor effect on the addition of nano-scale $CoCr_2O_4$ and its morphology. The mixture was then elevated to temperatures between 250 and 300 °C during the continuous agitation of the mixture at 200 rpm for 5–10 min. The solution then disintegrated as a result of its inherent self-ignition, foaming, and settling. Cobalt-chromite nanoparticles had been ball-milled to a fine mesh as a final phase. Fig. 3 depicts the synthesis procedure for the production of cobalt chromite nanoadditives.

2.3. Fuel characteristics and property measurement

Our previous research (Ramalingam et al., 2020) described the FTIR and GCMS analyses of citronella fuel. Figs. 4 and 5 present the outcomes of the FTIR and GCMS analyses (Krishnamoorthy et al., 2020). also describes the properties of synthesized cobalt chromite nanoadditives. Figs. 6, 7, and 8 depict the results of SEM, XRD, and EDX, respectively.

2.3.1. XRD analysis

X-ray diffraction (XRD) was used to determine the crystal structure and phase identification of nanocobalt chromite. To conform to and validate the material's crystal structure, the test is rendered as an image. On an X-ray diffractometer, copper was used as the target material (Cu K diffraction source) to study a sample of nanocobalt chromite complex. The observed and simulated CoCr2O4 patterns are depicted in Fig. 6. It is stated that the prepared cobalt-chromite compound's output closely resembles the simulation's output. Because Cr2O3 (@) is a screening impurity phase near 33 °C, the single-step solution combustion-

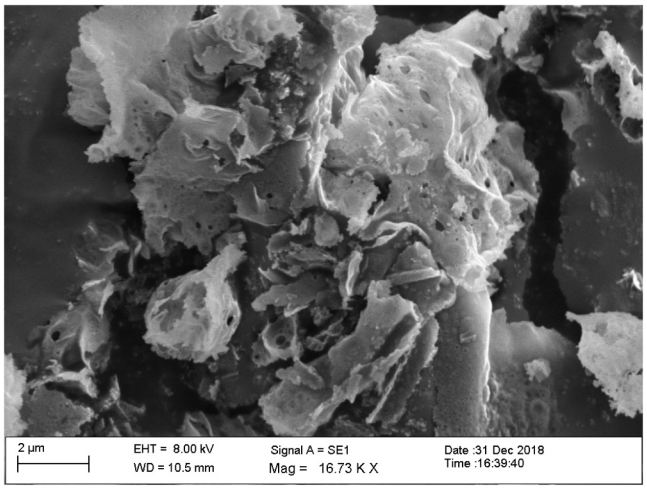

Fig. 6. SEM analysis of nanoparticle.

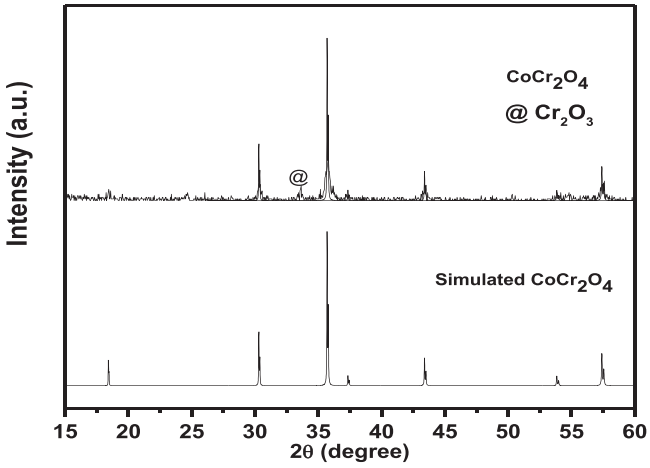

Fig. 7. XRD analysis of nanoparticle (Krishnamoorthy et al., 2020).

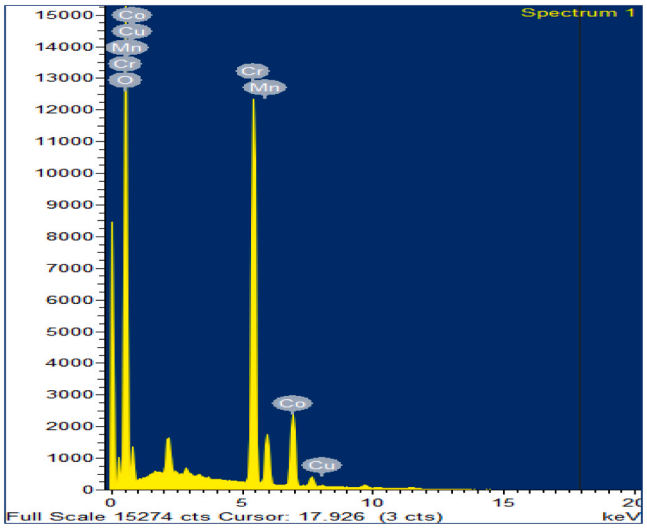

Fig. 8. EDX analysis of nanoparticle (Krishnamoorthy et al., 2020).

Table 1
Thermo-physicochemical properties of test fuels.

Properties	SDL	CGO	LFO	LFCO	NFCO
Calorific Value (MJ/kg)	44.1 ± 0.05	38 ± 0.05	28 ± 0.05	34 ± 0.05	36 ± 0.05
Cetane number	47 ± 0.03	55 ± 0.03	35 ± 0.03	38 ± 0.03	37 ± 0.03
Kinematic Viscosity (cSt)	2.9 ± 0.03	4.2 ± 0.03	4.3 ± 0.03	1.5 ± 0.03	1.2 ± 0.03
Flash Pt (°C)	66 ± 0.02	52 ± 0.02	85 ± 0.02	75 ± 0.02	71 ± 0.02
Density (kg/m^3)	820 ± 0.04	900 ± 0.04	907 ± 0.04	902 ± 0.04	904 ± 0.04

combustion synthesis does not make a pure phase of CoCr2O4. This is because a lot of Cr ions are quickly oxidized to form Cr2O3 precipitate when a lot of Cr ions are present. The crystallite size of the prepared cobalt chromite was determined to be 22 nanometers using the Scherrer formula:

$$D_P = \frac{0.94\lambda}{\beta_{\frac{1}{2}} \cos\theta} \quad (1)$$

where, D_p = crystallite's size in nm, Θ = degree theta and β radian.

The crystalline size was calculated by using the Debye Scherrer equation, $D = K\lambda / \beta\cos\theta$, crystalline size of this nanoparticle is 40 nm at 36 degrees and 39 nm at 31 degrees. The maximum 2θ values are observed at 36 and 31, and the corresponding intensities are 2759 and 1289, respectively. Therefore, the crystallinity index of this material is 54%, which is measured from $C.I = ((I_{max} - I_{min})/I_{max})$.

2.3.2. SEM analysis

An elemental analysis of the produced cobalt-chromite compound was performed using SEM microscopy. Fig. 7 depicts the SEM image obtained with an X-ray spectrometer and SEM analyzer at magnifications between 20,000 and 1,67,000. The experimental investigation was conducted at 8000 kV, and the results revealed a remarkable variety of porous particles. In contrast, the results indicate that when cobalt nanoparticles were oxidized from Cr to Cr2O3, their morphology changed substantially. An intermolecular chemical reduction of the cobalt complex leads to the formation of nanoscale particles in the new particles.

2.3.3. EDX

From the standpoint of energy composition, the mass of a substance that permits the formation of crystallites is relatively average. Fig. 8 shows the energy dispersive X-ray (EDX) spectrum of the compound made from cobalt and chromium. This shows that the cobalt, chromium, and oxygen parts are there. The collected data demonstrates conclusively that the manufactured CoCr2O4 composition is free of impurities.

2.3.4. Thermo-physicochemical properties

The thermo-physicochemical properties of test fuels are displayed in Table 1. The calorific value of a fuel sample was determined using a boom calorimeter (Athena Technology, India). The calorific value quantifies the quantity of energy released when one unit of fuel burns in oxygen. In order to measure heat according to ASTM D5865, a measured sample of fuel is completely consumed in an explosive calorimeter. Using an instrument for fuel ignition, the cetane number of the fuel sample was measured. The cetane number (CN) is a measurement of a fuel's combustion condition or ignition delay. This instrument employs a more uncomplicated and reliable method for measuring CN than the CFR cetane engine. To detect CN in accordance with ASTM D613, a constant volume of fuel is introduced into a combustion chamber at approximately 575 °C.

A viscometer measures a fluid's viscosity (resistance to internal flow). Determine the time required for the heated water to elevate the

Table 2
Test fuel matrix.

SI No	Test Name	Fuel	% Nano additive	Load
1.	SDL	100% Diesel	Nil	0–100%
2.	CGO	100% Citronella oil	Nil	0–100%
3.	LFO	100% Waste leather fat oil	Nil	0–100%
4.	LFCO	50% Waste leather fat oil +50% Citronella oil	Nil	0–100%
5.	NFCO	50% Waste leather fat oil +50% Citronella oil	100 ppm	0–100%

*Injection timing 23bTDC, Injection Pressure 200 bar.

oil's temperature to the point where the conduit can be sealed. Remove the seal when it reaches the end and time how long it takes to descend. The longer it takes for oil to ascend and descend, the greater its viscosity. The measurements were conducted according to ASTM D445 standards.

A device called a flash point analyzer is used to determine the flash point of a sample, or the temperature at which the sample vaporizes into a different compositional state that can be ignited in the atmosphere. The oil sample is placed in an open metal container for this procedure. The oil is then heated at a predetermined rate while maintaining a continuous, minute pilot flame (igniter) This continues until a detonation occurs. The temperature is then used to determine the oil's flash point. The measurements were carried out per ASTM D93.

Using the unitor density meter, which measures fuel density by lowering a hydrometer into heated oil, the density of the fuel sample was determined. The density of an object or substance is equal to its mass, m, divided by its volume, V, or m/V. The measurements were carried out per ASTM D1298.

2.4. Test fuel matrix

Diesel was utilized to evaluate the efficacy of four different combinations, including lather fat oil (LFO), citronella grass oil (CGO), a mixture of leather fat oil and citronella grass oil (LFCO), and a nano-additive containing a mixture of lather fat oil and citronella grass oil (NFCO). The comprehensive test matrix is shown in Table 2.

2.5. Engine matrix

A conventional one-cylinder Kirloskar diesel engine was utilized in the test. It features a 5.2-kW diesel engine with direct injection and naturally aspirated combustion. Air is brought into the cylinder through the inlet manifold during the vacuum stroke. Fig. 9 depicts the engine's schematic architecture, while Table 3 details the engine's precise specifications.

2.6. Experimental procedure

To prevent the engine from overheating, the flow of engine coolant and the level of lubrication lubricant were inspected before the

Table 3
Test Engine specification.

Make	Kirloskar TV-1
Type	4-stroke engine
Cooling	Water
Bae Engine Bore	86.6 mm
Bae Engine Stroke	112 mm
Compression ratio	17.6:1
Power Rated	5.1 kW
Speed	1500 rpm
IT	23 deg before TDC
Nozzle	0.3 mm and 3 nozzles
Bowl	Hemispherical

Table 4
Specifications of the emission analyzers.

S. No	Instrument	Type	Manufacturer	Measuring Range	standard error
1	Smoke meter	AVL Smoke meter	AVL India Pvt. Ltd.	0–100 HSU	±0.1
2	Five gas analyzer	Krypton 290 five gas analyzer	SMS Auto line Equipment's private limited	CO – (0–10%) CO_2 – (0–20%) HC – (0–10000 ppm) NO_X – (0–5000 ppm)	±0.1 ±0.1 ±0.05 ±0.02

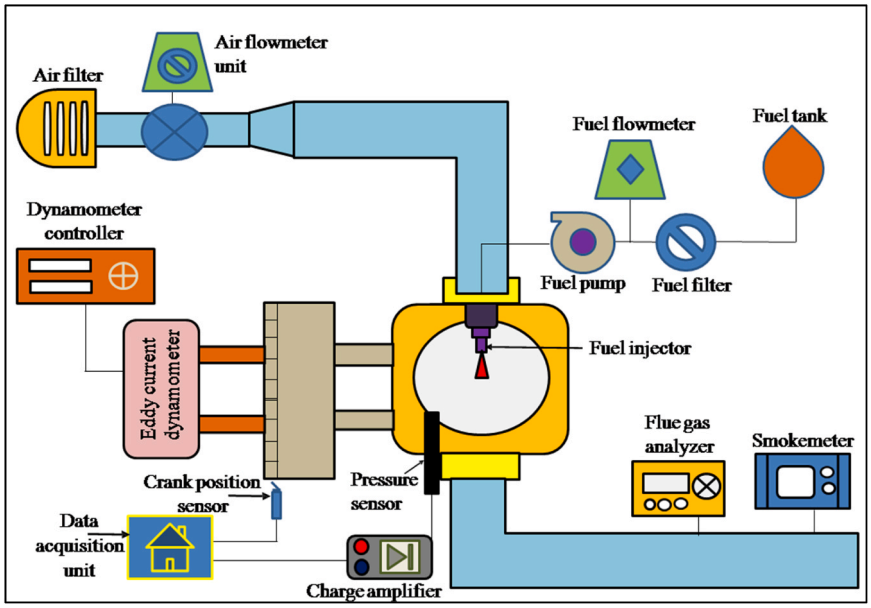

Fig. 9. Engine schematic setup.

Table 5
Ambiguity examination.

S.No	Measured parameters	Parentage uncertainty
1.	BTE	0.8%
2.	BSFC	0.6%
3.	Pressure	0.2%
4.	BP	0.4%
5.	Crank angle encoder	0.05%
6.	Engine Speed	0.1%
7.	Dynamometer Load	0.2%

experiment began. Initially, diesel was utilized under the following load conditions: 0%, 20%, 40%, 60%, 80%, and 100%. After initial readings were recorded, the diesel fuel was disposed of. The test engine was injected with various fuel mixtures to evaluate its performance and emissions. There were up to five repetitions of each experiment, regardless of the accuracy of the results. On the cylinder head, pressure sensors are installed to detect combustion characteristics. An AVL DI gas analyzer and a smoke analyzer are used to measure the exhaust emissions. In this investigation, the engine decarbonizing machine was utilized. For each fuel test, hydrogen and oxygen derived from water are circulated through an engine's air intake and exhaust systems to remove any residuals. Table 4 details the characteristics of the emission analyzers. Every measurement was logged, graphed, and analyzed.

2.7. Ambiguity examination

The most frequent causes of instrument errors are the instrument's condition, the surrounding environment, the method of observation, and the testing procedure. Variations in instrument manufacturers, calibration procedures, and data acquisition procedures may contribute to experimental uncertainty. Utilizing uncertainty analysis prevents fluctuations in intended experimental outcomes. Table 5 displays the ambiguity of various measuring devices and parameters.

$$\text{Total uncertainty (TU)} = \sqrt{(\text{Total performance deeds})^2 + (T\text{otal emission deeds})^2} \tag{2}$$

$$\text{TU} = \sqrt{(UC_{BTE})^2 + (UC_{BSEE})^2 + (UC_{HC})^2 + (UC_{CO})^2 + (UC_{NOx})^2 + (UC_{Smoke})^2} \tag{3}$$

TU $= \pm 1.378\%$.

2.8. ANN model

A highly complex neural network regulates, supports, determines, and correlates critical thought in the human brain. The human brain's neural network may be functionally equivalent to the ANN method. This method enables the investigation, simplification, and identification of infinite parameters. These neurons can be camouflaged more effectively as a large number of neurons. The outer layers, which correspond to synaptic weights, are linked to the concealed layers, and MSE aims to minimize the performance function. The previously mentioned MSE performs remarkably well in the background of operation and possesses properties that improve convexity, regularity, and differentiation. The selection of the learning algorithm to determine the transfer function is crucial in ANN. SCG, LM, RP, and BFGS are just a few of the available transfer function selection techniques. The previously mentioned MSE performs remarkably well in the background of operation and possesses properties that improve convexity, regularity, and differentiation. Important in ANN is the selection of the learning algorithm to determine the transfer function. SCG, LM, RP, and BFGS are just a few of the available transfer function selection techniques. According to Table 6, the configuration of the neural network for these parameters was 4–11–1, 4–11–1, 4–7–1, 4–7–1, 4–11–1, 4–11–1, and 4–11–1, respectively.

After cross-validating 70% of the trained network with 15% of the experimental data, the performance of the network was assessed using the remaining 15% of the data. To predict the performance of ANN models, the regression coefficient (R2) is considered. Using the MSE, RMSE, and MAPE values, the ANN model was built from the models proposed by different researchers. These fundamental equations are used to calculate the regression coefficient (R2) and the values used to build the ANN model:

$$R^2 = 1 - \frac{\sum_{i=1}^{n} (Ti - Oi)^2}{\sum_{i=1}^{n} Oi^2} \tag{4}$$

$$MAPE = \left\{ \frac{100}{n} \sum\nolimits_{i=1}^{n} \left(\frac{Ti - Oi}{Oi} \right) \right\} \tag{5}$$

$$MSE = \frac{1}{n} \left\{ \sum_{i=1}^{n} \left((Ti - Oi)^2 \right) \right\} \tag{6}$$

$$RMSE = \sqrt{\frac{1}{n} \sum_{i=1}^{n} (Ti - Oi)^2} \tag{7}$$

Utilizing R, MSE, and MAPE values as standard numerical indicators, the study is evaluated. Based on these metrics, iterations are either continued or terminated. If R is greater than 0.98 and MSE and MAPE are less than 0.001% and 5%, respectively, the ANN model will end its iteration. If these conditions are not met, the cycle will terminate after 100 iterations. Engine performance and emission characteristics are evaluated using an ANN model. Seven outputs, including HC, CO, CO2, NOx, and smoke opacity (emission parameters), as well as BTE and BSFC (performance parameters), were generated by the ANN model, which was constructed using two input parameters. Fig. 10 depicts the ANN model's configuration.

3. Result and discussion

3.1. BTE vs. BMEP

The BTE is used to evaluate the engine's ability to convert thermal energy from the fuel supply into mechanical work. The cetane number, heat content, and viscosity are the principal factors that have a significant impact on the outcomes of BTE (Erdiwansyah et al., 2020; Ramalingam et al., 2022). Fig. 11 depicts the disparity between the BTE for various test fuels at different BMEPs. Diesel fuel had a higher BTE than other mixtures, with NFCO being the blend that was closest to diesel. It is evident due to the lower energy content of CGO, LFCO, and LFO. Diesel has a maximal BTE of 32.39%, 0.60 points higher than NFCO (31.7%). The BTE for mixtures of CGO, LFCO, and LFO is 30.80%, 30.09%, and 28.80%, respectively. According to the results, NFCO was determined to be the optimal blend. This may be a result of the high ratio of nano-additives' surface area to volume and the presence of oxygen in citronella leather fat oil. Due to the low energy content and increased viscosity of the LFO, its BTE was minimal. These clarifications align with Vellaiyan's (Vellaiyan, 2023) findings from 2023. Due to its decreased energy content and increased viscosity, he determined that residual biodiesel from a lather factory contained minimal BTE. The NFCO was selected as the finest alternative to diesel fuel overall. The BTE was determined by applying the following equations:

$$BTE = \frac{BP}{TFC \times CV} (\%) \tag{8}$$

$$BP = \frac{2\pi NT}{60} \times S \quad (kW) \tag{9}$$

$$TFC = \frac{\rho \times \nu}{t} (g/s) \tag{10}$$

Table 6
Prediction accuracy value for BTE, BSEC, CO, CO_2, HC, NOx and Smoke using different training algorithm.

Learning algorithm	Network structure	Predication Accuracy		Predication Accuracy		Predication Accuracy		Predication Accuracy		Predication Accuracy		Predication Accuracy		Predication Accuracy	
		BTE		BSEC		CO		CO_2		HC		NOx		SMOKE	
		Training set	Testing set	Training set	Testing set	Training set	Testing set	Training set	Testing set	Training set	Testing set	Training set	Testing set	Training set	Testing set
SCG	4–5–1	9.42	97.34	98.12	96.78	95.69	92.99	98.69	93.69	96.86	94.89	98.26	95.78	91.99	94.76
SCG	4–6–1	96.52	94.23	99.23	95.86	95.78	93.06	95.23	92.45	95.23	95.67	95.48	94.76	2.85	93.88
SCG	4–7–1	98.23	96.31	97.36	94.78	95.46	91.29	96.79	89.96	94.78	93.85	89.56	93.28	93.48	92.79
SCG	4–8–1	97.65	95.76	96.59	94.62	94.89	90.26	97.23	88.42	93.86	92.89	88.79	91.29	94.82	91.99
SCG	4–9–1	95.46	97.25	99.29	94.78	97.88	94.65	95.69	89.69	95.99	96.88	93.68	93.68	93.48	90.82
SCG	4–10–1	98.74	96.88	98.67	93.78	96.28	93.08	94.44	90.36	97.89	95.99	94.59	92.79	96.85	91.79
SCG	4–11–1	99.22	98.40	99.36	97.99	95.78	93.62	93.69	91.36	95.62	94.89	96.89	93.18	95.37	93.89
LM	4–5–1	98.74	91.34	98.16	96.99	1.69	91.28	99.01	92.63	94.78	93.69	92.89	94.56	94.99	94.79
LM	4–6–1	98.23	94.56	99.09	97.12	94.78	92.99	98.62	93.96	96.78	94.99	97.89	96.01	95.68	93.49
LM	4–7–1	97.26	95.76	99.76	97.09	92.69	93.67	97.25	94.99	93.79	95.62	95.28	95.78	96.31	92.88
LM	4–8–1	99.03	96.45	96.65	97.86	99.01	91.99	95.23	92.78	96.88	93.89	96.18	94.99	95.08	91.99
LM	4–9–1	98.26	97.23	95.56	97.28	98.23	91.99	94.62	91.78	95.36	91.69	97.29	95.62	94.78	93.45
LM	4–10–1	98.76	96.78	95.99	95.23	97.62	90.68	93.26	90.78	94.78	92.59	94.44	94.78	96.47	94.89
LM	4–11–1	97.99	97.99	96.39	92.89	97.23	92.73	91.09	93.69	91.99	93.69	94.59	96.78	95.23	92.99
RP	4–5–1	98.23	98.06	99.08	91.78	93.26	92.69	96.28	94.01	96.88	95.78	98.89	95.29	98.72	94.39
RP	4–6–1	98.65	95.69	97.69	96.25	94.28	90.88	95.78	93.65	93.89	96.19	97.48	94.88	96.48	94.96
RP	4–7–1	99.14	94.78	98.07	93.72	95.08	90.70	94.99	92.99	92.74	97.02	93.48	95.38	95.48	92.99
RP	4–8–1	97.69	97.58	94.67	92.22	91.09	91.29	93.69	91.99	89.99	96.78	89.98	94.81	94.62	93.46
RP	4–9–1	97.12	96.69	92.69	91.11	91.69	92.39	92.68	90.28	88.69	95.28	88.28	89.62	92.78	94.86
RP	4–10–1	95.69	98.12	98.04	96.66	92.89	93.39	95.62	92.37	87.52	96.89	92.57	89.88	93.48	94.29
RP	4–11–1	99.74	93.39	92.26	96.28	93.66	90.88	94.78	91.73	98.72	97.86	93.58	91.29	96.49	95.06
BFGS	4–5–1	95.59	96.27	95.78	95.55	94.69	89.26	96.45	92.68	97.59	94.72	94.78	95.38	95.78	93.78
BFGS	4–6–1	96.99	91.99	94.37	94.44	95.61	88.16	93.69	93.33	94.63	96.19	95.38	94.80	96.18	91.11
BFGS	4–7–1	98.76	96.09	98.78	93.39	93.78	88.23	95.85	94.08	93.78	95.89	96.48	95.99	97.28	90.79
BFGS	4–8–1	99.03	96.79	96.78	97.01	95.29	88.92	96.69	92.99	95.85	97.48	96.17	96.30	96.18	92.86
BFGS	4–9–1	98.89	97.77	95.78	96.06	93.78	87.79	97.26	93.99	92.79	93.89	95.27	89.99	94.49	94.99
BFGS	4–10–1	97.66	98.07	94.23	95.29	97.28	86.29	93.69	91.28	91.99	92.59	96.47	89.96	93.18	93.49
BFGS	4–11–1	98.99	96.08	96.78	94.24	94.09	85.29	94.99	92.78	96.45	94.89	94.61	88.99	88.96	95.89

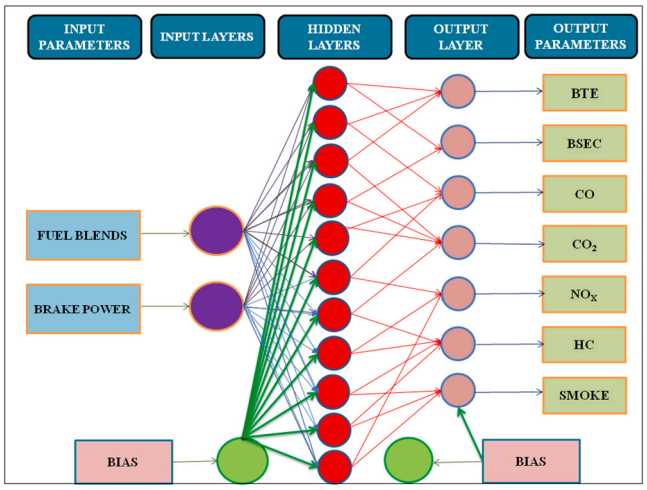

Fig. 10. Configuration of ANN model.

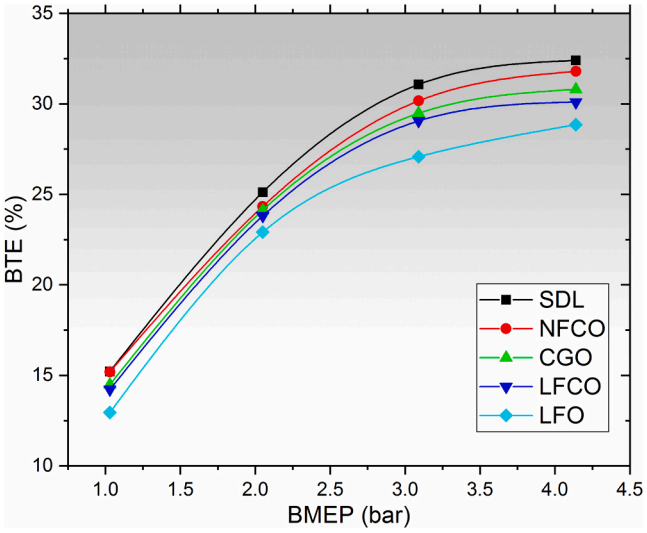

Fig. 11. BTE Vs BMEP.

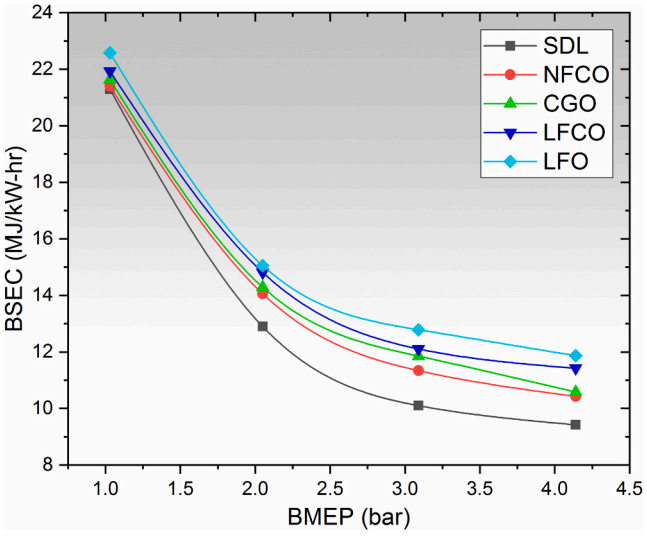

Fig. 12. BSEC Vs BMEP.

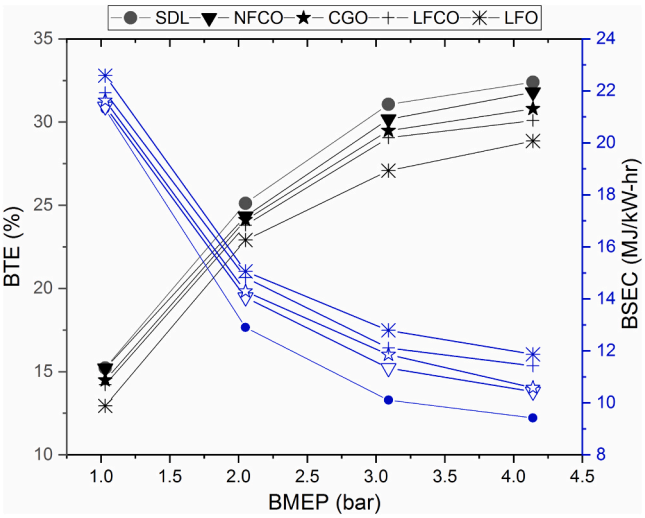

Fig. 13. BTE & BSEC Vs BMEP.

3.2. *BSEC vs. BMEP*

BSEC is the quantity of energy a motor needs to generate one kilowatt-second of power (Vellaiyan and Amirthagadeswaran, 2020). The amount of energy that one hour's worth of petroleum combustion produces is known as BSEC. Fig. 12 depicts the disparity between the BSEC for different test fuels at different BMEPs. Diesel fuel had a higher BSEC than other mixtures, with NFCO having the closest BSEC to diesel. It is evident due to the lower energy content of CGO, LFCO, and LFO. These explanations are consistent with Devarajan Yuvarajan et al.'s (Devarajan et al., 2022b) findings from 2022. The authors determined that leather industry-derived fat oil required more energy than diesel. In addition, Krishnamoorthy et al. (2019) (Ramalingam et al., 2019) demonstrated that citronella oil consumed more energy than diesel, which may account for its lower energy content. This result trajectory mirrored that of BTE, as shown in Fig. 13 for BTE and BSEC. The lowest diesel BSEC is 9.42 MJ/kW-hr, which is 9% less than the NFCO value of 10.42 MJ/kW-hr. The BSECs of CGO, LFCO, and LFO compositions are 10.57, 11.42, and 11.86 MJ/kW/hr, respectively. This may be a result of the high ratio of nanoadditives' surface area to volume and the presence of oxygen in citronella leather fat oil (Vellaiyan Sureh, 2020). Based on the results, it was determined that NFCO was the optimal composition

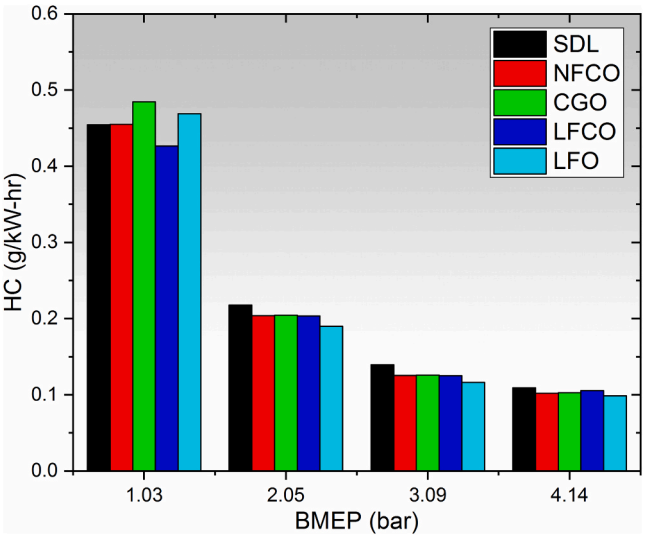

Fig. 14. HC Vs BMEP.

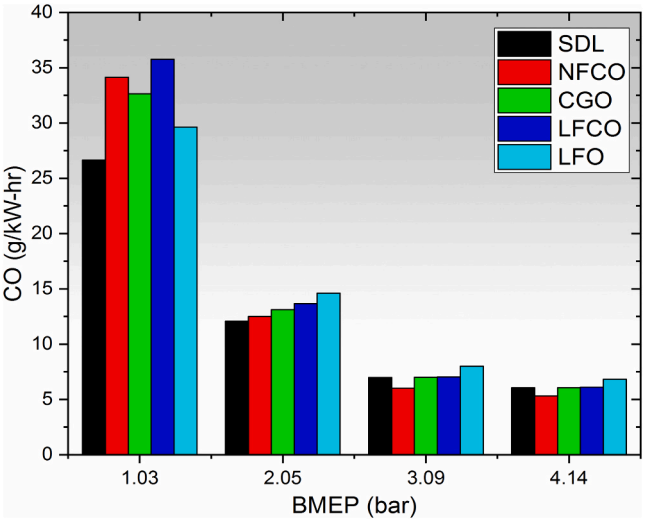

Fig. 15. CO Vs BMEP.

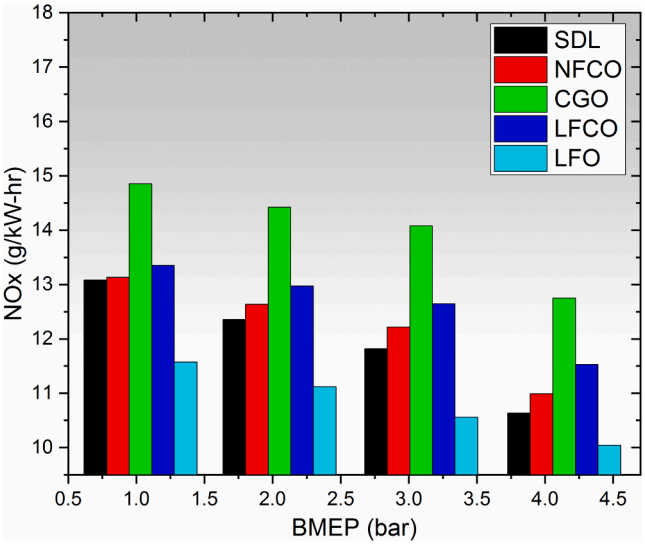

Fig. 16. NOx vs. BMEP.

due to its renewability, affordability, and accessibility. The BSEC was computed using the following equation (Eq. 11).

$$BSEC = \frac{TFC \times 3600}{BP} \times CV(MJ/kW - hr) \quad (11)$$

3.3. HC vs. BMEP

According to standard test procedures, exhaust gas emissions (CO, HC, CO2, and NOx) are calculated in parts per million (PPM) and converted to grams per kilowatt-hour (g/kW-h). Typically, the amount of hydrocarbons (HC) in tailpipe emissions depends on the characteristics of the fuel and the engine's operating conditions (Asaithambi et al., 2020). Fig. 14 depicts the variation in HC for various test fuels at different BMEPs. Due to a decline in volumetric efficiency and an increase in fuel accumulation, the amount of hydrocarbons in exhaust emissions has increased with increasing engine load (Vellaiyan et al., 2022a). As diesel contains no oxygen, it emits significantly more hydrocarbons than biofuel mixtures. Moreover, it has been found that biofuel mixtures only reduce HC emissions under moderate and heavier loads. It may be a result of faster mixing and evaporation rates as well as the burn procedure being completed within the allotted time. However, the biofuel compound contained more oxygen. According to Dhinesh, et al. (2018a) and Dhinesh et al. (2018b), these explanations are dependable. Due to the presence of oxygen, the authors reported that all lemongrass oils had lower HC emissions than diesel. The HC was overall lower. Diesel's HC content is 11% greater than that of LFO (0.098 g/kW-h). HCs for NFCO, CGO, and LFCO at maximum load are 0.102 g/kW-hr, 0.101 g/kW-hr, and 0.105 g/kW-hr, respectively. Surface tension and propellant viscosity are also crucial to the blending and atomization processes. They reduce the size of the particles, and rapid evaporation completely consumes the fuel within the cylinder, reducing HC emissions (Devarajan et al., 2022c).

3.4. CO vs. BMEP

Lack of oxygen or air in the combustion chamber is the primary cause of CO emissions, which are simply a byproduct of the intermediate zone. CO is an odorless, colorless, and toxic gas (Vellaiyan et al., 2022b). Fig. 15 depicts the difference in CO for various test fuels at different BMEPs. As the BMEP of the engine decreases, it is evident that the CO value rises; this may be due to high fuel accumulation and a lower cylinder temperature, which leads to incomplete combustion (Gurusamy et al., 2023). The lack of oxygen may explain why diesel produces more carbon monoxide than biofuel mixtures. Diesel has 15% higher CO emissions than NFCO (5.30 g/kW-hour). At full capacity, CGO, LFCO, and LFO emit 6.06 g/kW-hr, 6.75 g/kW-hr, and 6.93 g/kW-hr of CO, respectively. Ramalingam et al. (2023) ensure the accuracy of these annotations. They found that turpentine oil biofuel contained less carbon monoxide (CO), which may explain its higher oxygen (O2) content and efficient combustion. CI engines that use any oxygenated fuel, such as alcohol, biofuel, methyl ester, or enhanced viscosity fuel, reduce CO enrichment, according to multiple studies.

3.5. NOx vs. BMEP

NOx production typically occurs at elevated temperatures. Nitrogen and oxygen react within the cylinder at elevated temperatures to form NOx. The NOx production rate increases in stoichiometric conditions (Devarajan et al., 2022d). Fig. 16 depicts the variation in NOx for several test fuels at varying BMEPs. Due to diesel's low O2 concentration, it emits substantially less NOx than biofuel blends. The complete biofuel mixture, excluding LFO, produced more NOx than diesel due to its higher O2 content, which increases the peak combustion temperature. Due to rapid combustion, the thermal energy from the previous cycle, and the availability of oxygen, NOx emissions from a biofuel blend increase as engine load increases (Muthuraman and NanthagopalKasianantham, 2023). Diesel has 20% lower NOx emissions than CGO (12.75 g/kW-hour). NOx emissions at maximal load for NFCO, LFCO, and LFO are 10.96 g/kW-hr, 11.53 g/kW-hr, and 10.04 g/kW-hr, respectively. Less NOx emissions were detected with LFO fuel, which may indicate incomplete combustion. On the other hand, NFCO produced less NOx, which may have been due to the presence of nanoparticles. These explanations are irrefutable, according to Suresh (Vellaiyan et al., 2023). He determined that the biodiesel mixture containing titanium oxide reduced NOx emissions more than diesel. The NFCO was selected as the most effective alternative to diesel engines for reducing NOx emissions. This may be a result of the high ratio of nanoadditives' surface area to volume and the presence of oxygen in citronella leather fat oil.

3.6. CO_2 vs. BMEP

CO_2 is one of the primary causes of greenhouse gas (GHG) emissions, as it is the byproduct of complete combustion. It is indispensable for the growth and photosynthesis of plants and vegetation. When burning fossil fuels, carbon atoms are released into the atmosphere, causing CO_2 levels to rise; however, when burning biofuels derived from plants and

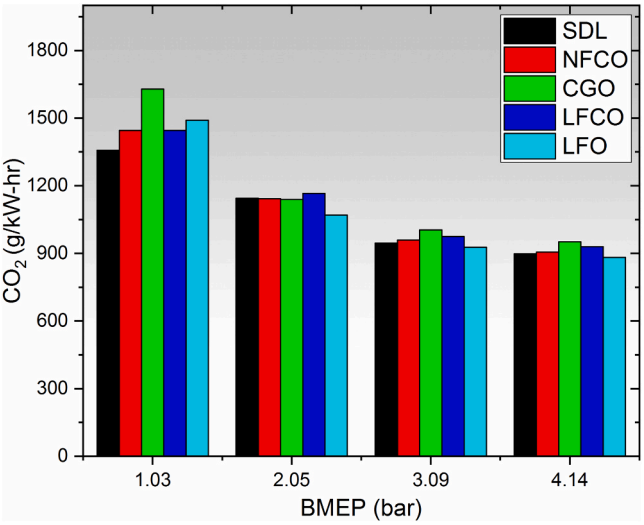

Fig. 17. CO_2 Vs BMEP.

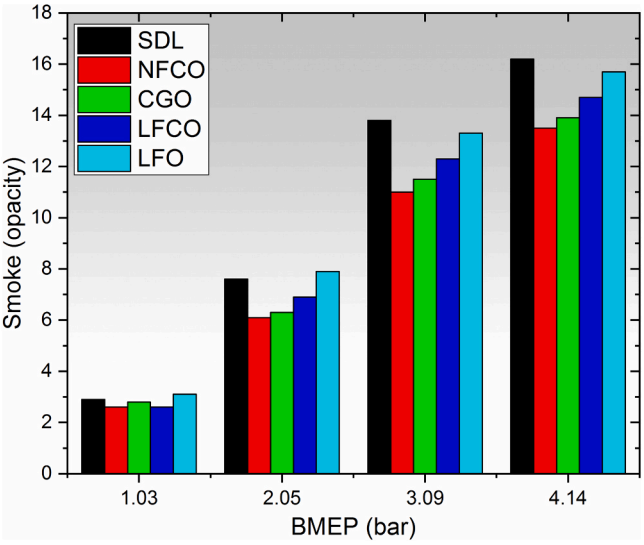

Fig. 18. Smoke Vs BMEP.

trees, CO_2 is recirculated rather than rising (Muthuraman and NanthagopalKasianantham, 2023; Vellaiyan et al., 2023). Fig. 17 depicts the variation in CO_2 for different test fuels at varying BMEPs. The trend resulted in less CO_2 formation as the burden increased, as depicted by the graph. Diesel emits 5% less CO_2 per kilowatt-hour than CGO (951.40 g/kW-hr). At full load, NFCO, LFCO, and LFO emit 905.4 g/kW-hr, 929.23 g/kW-hr, and 881.90 g/kW-hr of CO_2, respectively. According to the results, LFO fuel emitted less CO_2, which may be the cause of incomplete combustion. NFCO, however, produced more CO_2 than NFCO. Suresh V. et al. consistently provide these explanations. He determined that soybean biodiesel mixed with zirconium oxide produced less carbon dioxide than soybean biodiesel alone. This may be due to the nanofluid's high surface-to-volume ratio.

3.7. Smoke vs. BMEP

Fig. 18 depicts the variation in fumes produced by various test fuels with differing BMEP. The amount of oxygen present in the test propellant has a significant impact on the production of smoke. In other words, there is a strong association between smoke emissions and fuel mixture (Okolie et al., 2022). It is evident at maximum capacity that smoke opacity in exhaust emissions increases as load increases. Diesel emits significantly more vapor than biofuel blends, which is likely due to diesel's low oxygen content. In contrast to diesel, the complete biofuel mixture produced less smoke due to its lower aromatic content, lower C/H ratio, and higher oxygen content, which enhance combustion and fuel oxidation (Gad et al., 2021). Because NFCO, CGO, LFCO, and LFO contain more oxygen than NFCO, CGO, and LFO, diesel fuel is reported to produce more smoke than other mixtures. These explanations align with previous findings (Devarajan et al., 2022d; Vellaiyan et al., 2023). The maximal smoke level of diesel is 16.2, which is 20% higher than NFCO (13.5). The smoke for CGO, LFCO, and LFO mixtures is 13, 9, and 15, respectively. According to the results, NFCO was determined to be the optimal blend. This may be a result of the high ratio of nano-additives' surface area to volume and the presence of oxygen in citronella leather fat oil.

3.8. Prediction of engine behaviour by ANN model

In this study of prediction, ANN models are used to predict nonlinear issues. Using four distinct fuel compositions, including lubrication fat oil (LFO), citronella grass oil (CGO), a combination of leather fat oil and citronella grass oil (LFCGO), and a combination of leather fat oil and citronella grass oil containing nanoadditives The model is also used to determine engine performance and emission limitations. The created ANN model is straightforward and reliable, and there are available prediction toolboxes.

The two input parameters of the MATLAB network are the brake power and the fuel mixture, and the seven output parameters are NOX, CO, HC, CO2, haze, BTE, and BSEC. Based on data from test runs, the diesel engine prediction model network powered four distinct fuel blends: leather fat oil (LFO), citronella grass oil (CGO), a combination of leather fat oil and citronella grass oil (LFCGO), and a combination of leather fat oil and citronella grass oil with nano additives. The performance of the constructed model was evaluated using a total of 30 test patterns, of which 80% (24 patterns) were selected at random for training and 20% (6 patterns) were designated for testing and validation.

To ensure the network's success, the best learning strategies and hidden neuron (HN) counts must be selected. In this study of prediction, the MSE results and an R-value report were used to determine the optimal learning algorithms for the architecture and number of HN, which were then subjected to a series of trial-and-error experiments (Samuel et al., 2021). An increase in R and a decrease in MSE often determine the optimal configuration of a neural network for the number of HNs and learning techniques. R and RMSE were found to have the highest and lowest values, respectively, in this study of prediction (Olusegun et al., 2016). On the basis of these values, it was determined that the LM learning algorithms and eleven hidden neuron counts were the most effective solutions (Mokashi et al., 2021), and these values were recorded in Tables 7 and 8. Fig. 19 illustrates the disparity between ANN predictions and experimental results.

RMSE values for BTE, BSEC, CO, CO2, HC, NOx, and smoke are respectively 0.405, 0.026, 0.0206, 0.0158, 0.0195, and 2.685. R-values for BTE, BSEC, CO, CO2, HC, NOx, and pollution are 0.9965, 0.9889, 0.9784, 0.95, 0.9076, and 0.9849, respectively. Remember that the RMSE value represents the quantity of error encountered during the process of learning. The MAPE values for BTE, BSEC, CO, CO2, HC, NOx, and pollution are 1.15%, 0.87%, 3.17%, 2.62%, 4.26%, 1.68%, and 0.97%, respectively. According to the presently developed ANN model, the relative error will be less than 4%, which is within the acceptable range. According to the error analysis, the data correspond to the experimental analysis and ANN forecasts. In addition to the information presented in Table 8, the R-value ranges between 0.9076 and 9965. The MAPE values vary between 0.98% and 4.26%. This is extremely trivial. Evidently, the constructed ANN model is a potent tool with the ability to predict engine performance and emission parameters that are extremely

Table 7
Summary of statistical value for BTE, BSEC, CO, CO_2, HC, NOx and Smoke using different training algorithms.

Parameters	Learning algorithm	Network structure	Training Set			Testing set		
			R	RMSE	MAPE	R	RMSE	MAPE (%)
BTE	SCG	4–11–1	0.9992	0.401	0.99	0.9965	0.405	1.15
	LM	4–11–1	0.9991	0.389	1.25	0.9952	0.459	2.15
	RP	4–5–1	0.9976	0.372	2.84	0.9931	0.526	2.38
	BFGS	4–10–1	0.9823	0.402	3.12	0.9960	0.428	3.12
BSEC	SCG	4–11–1	0.9998	0.019	0.65	0.989	0.026	0.87
	LM	4–8–1	0.9986	0.013	0.79	0.972	0.031	1.38
	RP	4–10–1	0.9972	0.021	0.83	0.979	0.038	2.89
	BFGS	4–8–1	0.9991	0.018	1.69	0.983	0.046	4.18
CO	SCG	4–9–1	0.9812	0.0200	2.38	0.9621	0.0228	3.89
	LM	4–7–1	0.9991	0.0201	2.18	0.9784	0.0206	3.17
	RP	4–5–1	0.9745	0.0189	2.54	0.9542	0.0399	4.10
	BFGS	4–5–1	0.9789	0.0179	3.09	0.9432	0.123	2.99
CO_2	SCG	4–5–1	0.976	0.0099	2.94	0.941	0.286	3.99
	LM	4–7–1	0.998	0.0151	1.82	0.955	0.0158	2.60
	RP	4–5–1	0.956	0.0139	3.08	0.948	0.0458	2.88
	BFGS	4–7–1	0.948	0.0128	1.99	0.896	0.0389	2.92
HC	SCG	4–9–1	0.9681	0.0154	3.29	0.9034	0.0996	4.58
	LM	4–7–1	0.9482	0.0168	2.89	0.8742	0.0648	4.37
	RP	4–11–1	0.9952	0.0182	2.48	0.9076	0.0195	4.26
	BFGS	4–8–1	0.9901	0.0159	4.01	0.8894	0.0784	4.84
NOx	SCG	4–5–1	0.9894	2.318	2.35	0.9812	2.998	2.47
	LM	4–11–1	0.9919	2.459	0.89	0.9849	2.685	1.69
	RP	4–7–1	0.9689	2.999	1.89	0.9765	2.798	1.99
	BFGS	4–8–1	0.9789	2.267	2.98	0.9661	3.128	3.28
SMOKE	SCG	4–5–1	0.9802	0.489	2.08	0.976	0.512	2.99
	LM	4–10–1	0.9758	0.512	1.89	0.990	0.489	2.84
	RP	4–11–1	0.9874	0.477	0.99	0.985	0.389	1.23
	BFGS	4–11–1	0.9992	0.189	0.65	0.993	0.333	0.98

Table 8
Summary of R, RMSE, and MAPE for BTE, BSEC, CO, CO_2, HC, NOx and Smoke using different training algorithms.

Output Parameters	Training algoritham	No of nureons in hidden layers	R (Pearson Product moment correlation)	RMSE (Root Mean squared Error)	MAPE (Mean Absoulte percentage Error)
BTE	SCG	11	0.9965	0.405	1.15%
BSEC	SCG	11	0.989	0.026	0.87%
CO	LM (LevenbergeMarquardt)	7	0.9784	0.0206	3.17%
CO_2	LM (LevenbergeMarquardt)	7	0.955	0.0158	2.60%
HC	RP	11	0.9076	0.0195	4.26%
Nox	LM (LevenbergeMarquardt)	11	0.9849	2.685	1.69%
Smoke	BFGS	11	0.993	0.333	0.98%

close to experimental results. The researcher emphasized and elaborated on how the ANN model reduces experimental cost, experimentation time, and analytical complexity. This type of prediction model is extremely useful for mapping the engine's output response, and it also assists the control system.

4. Conclusion

The production of biodiesel from waste has many advantages. It is beneficial for the environment because it facilitates the administration of waste, a task that is often difficult to execute. There is no competition between food and waste, so food prices will not be affected. Regarding carbon dioxide emissions, the use of organic waste should be weighed favourably. The examination of the obtained test results and the research conducted on a novel combination of leather fat oil, citronella oil, and cobalt chromite nanoadditives enabled the following conclusions:

- The NFCO blend provides better BTE and BSEC performance than other biofuel compositions. In addition, the NFCO blend's response to exhaust emission output was greener than conventional diesel.
- The developed ANN network was utilised to predict both performance and emission output responses, yielding commendable results, as evidenced by the fact that the value of R was increased to 97% for all output constraints.
- In addition, the ANN model is more accurate, with high R values ranging from (0.9076–0.9965) and low MAPE values ranging from (0.98%−4.26%).
- It is evident that the developed model is a useful instrument, as it has an excellent capacity to predict engine performance and produce results that are much closer to experimental findings.

The financial cost of incorporating nanoparticles, even though doing so efficiently enhances the overall combustion performance of the engine as well as the quality of the emissions produced, is a source of concern. In addition, nanoparticles that are released into the atmosphere present a risk to the surrounding environment. Nanoparticles that are both economical and friendly to the environment are necessary in this field. Future research should also establish an electrostatic precipitator for diesel engines to retain nanoparticles in the exhaust.

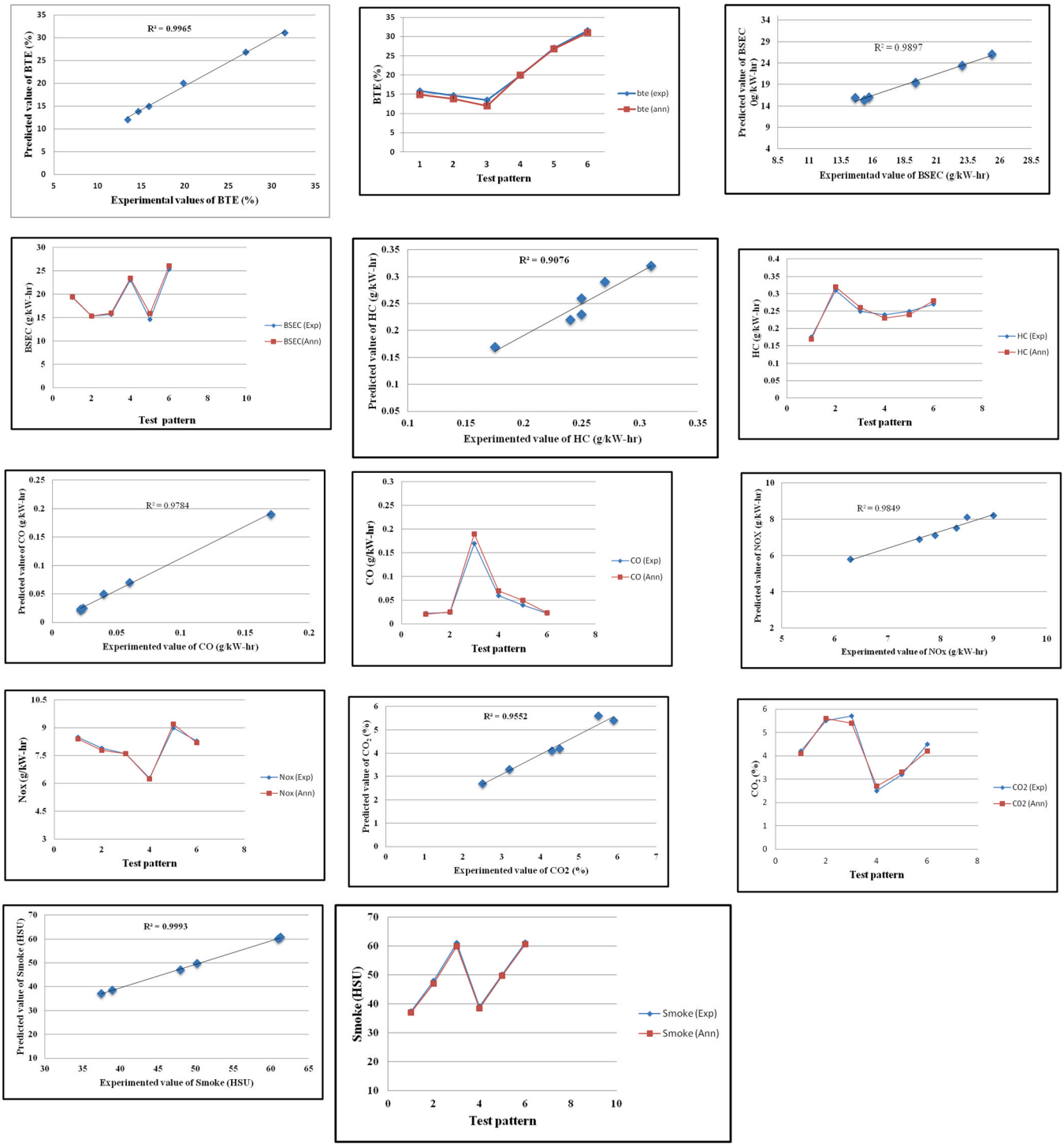

Fig. 19. Contrast between the ANN predictions and experimental results: (a) BTE; (b) BSEC; (c) HC; (d) CO; (e) NOx; (f) CO_2; and (g) NOx.

Declaration of Competing Interest

The authors declare that they have no known competing financial interests or personal relationships that could have appeared to influence the work reported in this paper.

Acknowledgements

The authors extend their appreciation to the Deanship of Scientific Research at King Khalid University for funding this work through large group Research Project under grant number RGP 2/45/44. The authors would like to express their heartful thanks to Dr S.Saravanan, Principal, CK College of Engineering and Technology, Cuddalore. Finally, the authors thanked Dr K. Annamalai, Professor, Department of automobile department, MIT, Anna University, Chromepet, and Chennai 44 for allowed to utilized his Engine Research Lab for this work.

Appendix 1

(a) Uncertainty calculation of performance parameter (BTE)

Let 'P' is the projected measurement, and A_1, A_2, … A_n are the independent parameters of 'P'. Now, the error of the 'P' is denoted by

$$P = f \quad (A_1, A_2, \ldots A_n) \tag{A1}$$

The uncertainty of 'P' is estimated by

$$\Delta P = \sqrt{\left(\frac{\partial P}{\partial A_1}.\Delta A_1\right)^2 + \left(\frac{\partial P}{\partial A_2}.\Delta A_2\right)^2 + \ldots. + \left(\frac{\partial P}{\partial A_n}.\Delta A_n\right)^2} \tag{A2}$$

The uncertainty of BTE was calculated as follows:

$$\Delta BTE = \sqrt{\left(\frac{\partial BTE}{\partial BP}.\Delta BP \quad\right)^2 + \left(\frac{\partial BTE}{\partial FC}.\Delta FC\right)^2 + \left(\frac{\partial BTE}{\partial CV}.\Delta CV \quad\right)^2} \tag{A3}$$

Sample calculation

$$BTE = f(TFC, BP) \tag{A4}$$

$$\frac{\partial BTE}{\partial BP} = \frac{3600 * 100}{0.246 * 44120} = 33.17$$

$$\frac{\partial BTE}{\partial TFC} = \frac{0.97 * 3600 * 100}{(0.246)^2 * 44.12} = 131.8$$

$$\Delta BTE = \sqrt{\left(\frac{\partial BTE}{\partial TFC}.\Delta TFC\right)^2 + \left(\frac{\partial BTE}{\partial BP}.\Delta BP\right)^2} \tag{A5}$$

$$\Delta BTE = \sqrt{(33.17 * 0.0077)^2 + (131.8 * 0.00286)^2} = 0.8$$

$$\Delta BTE = \pm 0.8$$

(b) Uncertainty calculation of fuel property (density)

Instrumental Uncertainty = ± 0.01 kg/m^3.

Calibration Uncertainty = ± 0.02 kg/m^3

$$Combined \quad Uncertainty = \sqrt{\text{Instrumental Uncertainty}^2 + \text{Calibration Uncertainty}^2} \tag{A6}$$

$$Combined \quad Uncertainty = \sqrt{0.01^2 + 0.02^2} = 0.022$$

$$\text{Expanded Uncertainty} = k * Combined \quad Uncertainty \tag{A7}$$

For a 95% confidence level, k value is about to 2. Hence, the expanded uncertainty of density is ±0.044.

References

Alptekin, Ertan, et al., 2015. Using waste animal fat based biodiesels–bioethanol–diesel fuel blends in a DI diesel engine. Fuel 157, 245–254.

Altun, S.şehmus, FevziYaşar, 2013. Biodiesel production from leather industry wastes as an alternative feedstock and its use in diesel engines. Energy Explor. Exploit 31 (5), 759–770.

Asaithambi, K., R. Krishnamoorthy, and Dhinesh Balasubramanian, 2020. A Comparative assessment of tailpipe emission characteristics on diesel engine using nanofluid with R-EGR setup. SAE Technical Paper. No. 2020–28-0442.

Ashok, B., et al., 2018. A novel study on the effect lemon peel oil as a fuel in CRDI engine at various injection strategies. Energy Convers. Manag. 172, 517–528.

Barrios, Carmen C., et al., 2014. Effects of animal fat based biodiesel on a TDI diesel engine performance, combustion characteristics and particle number and size distribution emissions. Fuel 117, 618–623.

Devan, P.K., Mahalakshmi, N.V., 2009. A study of the performance, emission and combustion characteristics of a compression ignition engine using methyl ester of paradise oil–eucalyptus oil blends. Appl. Energy 86 (5), 675–680.

Devarajan, Yuvarajan, et al., 2022a. Biofuel from leather waste fat to lower diesel engine emissions: valuable solution for lowering fossil fuel usage and perception on waste management. Process Saf. Environ. Prot. 165, 374–379.

Devarajan, Yuvarajan, et al., 2022b. Inedible oil feedstocks for biodiesel production: a review of production technologies and physicochemical properties. Sustain. Chem. Pharm. 30, 100840.

Devarajan, Yuvarajan, et al., 2022c. Evaluation of compression ignition engine ignition patterns fueled with dual fuels. Int. J. Green. Energy 19 (6), 676–684.

Devarajan, Yuvarajan, et al., 2022d. Biofuel from leather waste fat to lower diesel engine emissions: Valuable solution for lowering fossil fuel usage and perception on waste management. Process Saf. Environ. Prot. 165, 374–379.

Dhinesh, B., et al., 2018a. A numerical and experimental assessment of a coated diesel engine powered by high-performance nano biofuel. Energy Convers. Manag. 171, 815–824.

Dhinesh, B., Raj, Y.M., Kalaiselvan, C., KrishnaMoorthy, R., 2018b. A numerical and experimental assessment of a coated diesel engine powered by high-performance nano biofuel. Energy Convers. Manag. 171, 815–824.

Dubey, Pankaj, Gupta, Rajesh, 2017. Effects of dual bio-fuel (Jatropha biodiesel and turpentine oil) on a single cylinder naturally aspirated diesel engine without EGR. Appl. Therm. Eng. 115, 1137–1147.

Dubey, Pankaj, Gupta, Rajesh, 2018. Influences of dual bio-fuel (Jatropha biodiesel and turpentine oil) on single cylinder variable compression ratio diesel engine. Renew. Energy 115, 1294–1302.

Erdiwansyah, Erdiwansyah, et al., 2020. The effects of using diesel-citronella fuel blend on the emission and fuel consumption for single-cylinder diesel engine. J. Adv. Res. Fluid Mech. Therm. Sci. 74 (2), 1–15.

Gad, M.S., El-Shafay, A.S., Abu Hashish, H.M., 2021. Assessment of diesel engine performance, emissions and combustion characteristics burning biodiesel blends from jatropha seeds. Process Saf. Environ. Prot. 147, 518–526.

Gurusamy, Mahesh, et al., 2023. Optimization of process parameters to intensify the yield rate of biodiesel derived from waste and inedible Carthamus lanatus (L.) Boiss. seeds and examine the fuel properties with pre-heated water emulsion. Sustain. Chem. Pharm. 33, 101137.

Keskin, Ahmet, Şen, Mehmet, Emiroğlu, Alaattin Osman, 2020. Experimental studies on biodiesel production from leather industry waste fat and its effect on diesel engine characteristics. Fuel 276, 118000.

Krishnamoorthy, R., et al., 2020. Effect of cobalt chromite on the investigation of traditional CI engine powered with raw citronella fuel for the future sustainable renewable source. SAE Int. J. Adv. Curr. Pract. Mobil. 3 (2020–28-0445), 843–850.

Kurczyński, Dariusz, et al., 2022. Production and testing of butyl and methyl esters as new generation biodiesels from fatty wastes of the leather industry. Energy 15 (22), 8744.
Lapuerta, Magin, et al., 2009. Biodiesel from low-grade animal fats: diesel engine performance and emissions. Energy Fuels 23 (1), 121–129.
Lazaroiu, Gheorghe, et al., 2017. Solutions for energy recovery of animal waste from leather industry. Energy Convers. Manag. 149, 1085–1095.
Mokashi, I., Afzal, A., Khan, S.A., Abdullah, N.A., Bin Azami, M.H., Jilte, R.D., Samuel, O. D., 2021. Nusselt number analysis from a battery pack cooled by different fluids and multiple back-propagation modelling using feed-forward networks. Int. J. Therm. Sci., 106738 https://doi.org/10.1016/j.ijthermalsci.2020.106738.
Muthuraman, V.Shenbaga, and NanthagopalKasianantham , 2023. Valorization Opportunities and Adaptability Assessment of Algae Based Biofuels for Futuristic Sustainability. Process Saf. Environ. Prot.
Nachippan, N.Murugu, et al., 2022. Experimental assessment on characteristics of premixed charge compression ignition engine fueled with multi-walled carbon nanotube-included Tamanu methyl ester. Fuel 323, 124415.
Okolie, Jude A., et al., 2022. Waste biomass valorization for the production of biofuels and value-added products: a comprehensive review of thermochemical, biological and integrated processes. Process Saf. Environ. Prot. 159, 323–344.
Olusegun, D.S., Solomon, O.G., Suleiman, A.E., 2016. Optimization of coconut oil ethyl esters reaction variables and prediction model of its blends with diesel fuel for density and kinematic viscosity. Biofuels 7 (7), 1–13.
Parthasarathy, M., et al., 2020. Performance analysis of HCCI engine powered by tamanu methyl ester with various inlet air temperature and exhaust gas recirculation ratios. Fuel 282, 118833.
Parthasarathy, M., et al., 2021. Experimental investigation of strategies to enhance the homogeneous charge compression ignition engine characteristics powered by waste plastic oil. Energy Convers. Manag. 236, 114026.
Perumal Venkatesan, Elumalai, et al., 2019. Performance and emission reduction characteristics of cerium oxide nanoparticle-water emulsion biofuel in diesel engine with modified coated piston. Environ. Sci. Pollut. Res. 26, 27362–27371.
Ramalingam, Krishnamoorthy, et al., 2020. An assessment on production and engine characterization of a novel environment-friendly fuel. Fuel 279, 118558.
Ramalingam, Krishnamoorthy, et al., 2022. Assessment of CI engine performance and exhaust air quality outfitted with real-time emulsion fuel injection system. Sustainability 14 (9), 5313.
Ramalingam, Krishnamoorthy, et al. 2023. Challenges and Opportunities of Low Viscous Biofuel— A Prospective Review. ACS Omega.
Ramalingam, Krishnamoorthy, Kandasamy, Annamalai, Chellakumar, Paul James Thadhani Joshua Stephen, 2019. Production of eco-friendly fuel with the help of steam distillation from new plant source and the investigation of its influence of fuel injection strategy in diesel engine. Environ. Sci. Pollut. Res. 26, 15467–15480.
Ramalingam, KrishnaMoorthy, et al., 2018. An assessment of combustion, performance characteristics and emission control strategy by adding anti-oxidant additive in emulsified fuel. Atmos. Pollut. Res. 9 (5), 959–967.
Samuel, Olusegun D., et al., 2021. Modelling of Nicotiana Tabacum L. oil biodiesel production: comparison of ANN and ANFIS. Front. Energy Res. 8, 612165.
Senthilkumar, P.B., et al., 2022. The influence of exhaust gas recirculation on the characteristics of compression ignition engines powered by tamanu methyl ester. Int. J. Low. -Carbon Technol. 17, 856–869.
Senthur, N.S., et al., 2022. Influence of cobalt chromium nanoparticles in homogeneous charge compression ignition engine operated with citronella oil. Energy Sci. Eng. 10 (4), 1251–1263.
Simsek, Suleyman, Uslu, Samet, 2020. Comparative evaluation of the influence of waste vegetable oil and waste animal oil-based biodiesel on diesel engine performance and emissions. Fuel 280, 118613.
Sivalingam, Arularasu, et al., 2019. Citrullus colocynthis-an experimental investigation with enzymatic lipase based methyl esterified biodiesel. Heat. Mass Transf. 55, 3613–3631.
Subramani, Lingesan, et al., 2018. Novel Garcinia gummi-gutta methyl ester (GGME) as a potential alternative feedstock for existing unmodified DI diesel engine. Renew. Energy 125, 568–577.
Vellaiyan, Sureh, 2023. Production and characterization of Cymbopogon citratus biofuel and its optimization study for efficient and cleaner production blended with water and cetane improver: a response surface methodology approach. Fuel 351, 129000.
Vellaiyan, Suresh, 2020. Effect of cerium oxide nanoadditive on the working characteristics of water emulsified biodiesel fueled diesel engine: an experimental study. Therm. Sci. 24 (1 Part A), 231–241.
Vellaiyan, Suresh, et al., 2022a. Energy, environmental and economic assessment of waste-derived lemon peel oil intermingled with high intense water and cetane improver. Sustain. Energy Technol. Assess. 53, 102659.
Vellaiyan, Suresh, et al., 2022b. Water in waste-derived oil emulsion fuel with cetane improver: formulation, characterization and its optimization for efficient and cleaner production. Fuel Process. Technol. 228, 107141.
Vellaiyan, Suresh, et al., 2023. Optimisation of fuel modification parameters for efficient and greener energy from diesel engine powered by water-emulsified biodiesel with cetane improver. Case Stud. Therm. Eng., 103129
Vellaiyan, Suresh, Amirthagadeswaran, K.S., 2020. Compatibility test in a CI engine using lemon peel oil and water emulsion as fuel. Fuel 279, 118520.
Vellaiyan, Suresh, Partheeban, C.M.Anand, 2020. Combined effect of water emulsion and ZnO nanoparticle on emissions pattern of soybean biodiesel fuelled diesel engine. Renew. Energy 149, 1157–1166.
Vellaiyan, Suresh, Subbiah, Arunkumar, Chockalingam, Prabha, 2021. Effect of titanium dioxide nanoparticle as an additive on the working characteristics of biodiesel-water emulsion fuel blends. Energy Sources Part A 43 (9), 1087–1099.
Vellaiyan Sureh, 2020. Effect of cerium oxide nanoadditive on the working characteristics of water emulsified biodiesel fueled diesel engine: an experimental study. Therm. Sci. 24 (1 Part A), 231–241.
Vigneswaran, R., et al., 2018. Experimental investigation of unmodified diesel engine performance, combustion and emission with multipurpose additive along with water-in-diesel emulsion fuel. Energy Convers. Manag. 172, 370–380.